Remaining Useful Lifetime Estimation for Thermally Stressed Power MOSFETs Based on ON-State Resistance Variation

Serkan Dusmez, *Student Member, IEEE*, Hamit Duran, and Bilal Akin, *Senior Member, IEEE*

***Abstract*—The research on noninvasive incipient fault diagnosis of power converters is very critical to avoid strenuous periodic check-ups and costly interruptions. Thermal cycling is one of the main techniques to accelerate the package-related failure progress. In this paper, first, a custom designed accelerated aging platform that can expose multiple discrete power MOSFETs to thermal stress simultaneously is introduced. Based on the collected experimental data, the variation of the ON-state resistance is identified as the failure precursor, and an exponential degradation model that fits successfully with the experimental data are developed. The remaining useful lifetime (RUL) of degraded power MOSFETs is estimated through classical least-squares algorithm run on experimental data filtered by Kalman Filter which deals with the measurement noise and model uncertainties. The essential advantage of the proposed method is that it does not require junction temperature information. The RUL estimation with limited field data is demonstrated on a number of experimental results.**

***Index Terms*—Accelerated aging platform, fault diagnostics, Kalman filter (KF), ON-state resistance, power MOSFET, remaining useful lifetime (RUL), thermal cycling.**

I. Introduction

THE reliability of a power conversion system is mainly dictated by the failure rate of the electrolytic bus capacitor [1]–[3], and the power semiconductor switches [4]–[10]. In applications requiring higher reliability, electrolytic capacitors are replaced with film capacitors that exhibit lower equivalent series resistance. On the other hand, the power devices are subjected to various mechanical and electrical stresses, wear, and vibration in harsh environments that contribute to increased equipment failure rate. The dependence of switch reliability on the operating conditions has been widely discussed in the literature. It has been shown that the temperature swing resulting in extrinsic failure can have severe impact on the total lifetime of the switch [11]. Thus, developing prognosis tools is vital for the reliability of these systems.

The reliability of Si-based power semiconductor devices has been exhaustively researched on custom-designed accelerated test-beds. In general, power and thermal cycling tests are employed to realize and demonstrate thermal swing effects on the power devices [7], [9]–[13]. This type of accelerated test particularly propagates the package-related extrinsic failures. Majority of the studies evaluated the failure precursors of IGBTs. The major findings were variation in collector-emitter voltage [9], peak value of the collector-emitter ringing during turn-off [14], and gate-source threshold voltage [15]. In studies that focused on power MOSFETs, the reported failure precursor is the increased ON-state resistance that occurs due to the bond-wire degradation, gate-oxide degradation, and cracks and delamination in the die attach solder [11]–[13], [16].

Although the precursors have been well identified, there are a few studies that put effort on estimating the remaining useful lifetime (RUL) of power switches. The reported RUL methods are essentially either model based or data-driven approaches. In model-based approaches, typically, junction temperature information is obtained from the power losses and thermal impedance model of the switch, while temperature cycles are counted using algorithms such as rain-flow counting [17], [18]. The data-driven methods involve processing of experimental data to derive an empirical degradation model. In [19], relevance vector machine is used to train the degradation data of power MOSFETs to obtain representative vectors, which are fitted by a degradation model. A threshold value is defined and RUL is estimated using the proposed degradation model. In [16], Kalman filter (KF) and particle filter are proposed for failure prognosis; however, the details of the implementation have not been presented.

In this paper, a data-driven approach is presented. The experimental data are obtained through exhaustive tests and exponential empirical model is proposed to estimate the RUL of the switches. The empirical coefficients are found by least-squares method which uses the KF filtered data dealing with the model uncertainties and measurement noise. The basic advantage of this method is that it does not require junction temperature information, but it only requires ON-state resistance measurement that is quite practical to sense. The results are verified on a number of experimental data.

Manuscript received September 20, 2015; revised December 6, 2015; accepted January 1, 2016. Date of publication January 14, 2016; date of current version May 18, 2016. Paper 2015-IACC-0742.R1, presented at the 2015 IEEE Energy Conversion Conference and Exposition, Montreal, QC, Canada, September 20–24, and approved for publication in the IEEE TRANSACTIONS ON INDUSTRY APPLICATIONS by the Industrial Automation and Control Committee of the IEEE Industry Applications Society. This work was supported in part by the TXACE/SRC under Grant TASK 1836.154 and in part by the U.S. National Science Foundation under Grant 1454311.

S. Dusmez and B. Akin are with the Power Electronics and Drives Laboratory, Department of Electrical and Computer Science, The University of Texas at Dallas, Richardson, TX 75083 USA (e-mail: serkan.dusmez@utdallas.edu; bilal.akin@utdallas.edu).

H. Duran is with Texas Instruments, Dallas, TX 75080 USA (e-mail: h-duran@ti.com).

Color versions of one or more of the figures in this paper are available online at http://ieeexplore.ieee.org.

Digital Object Identifier 10.1109/TIA.2016.2518127

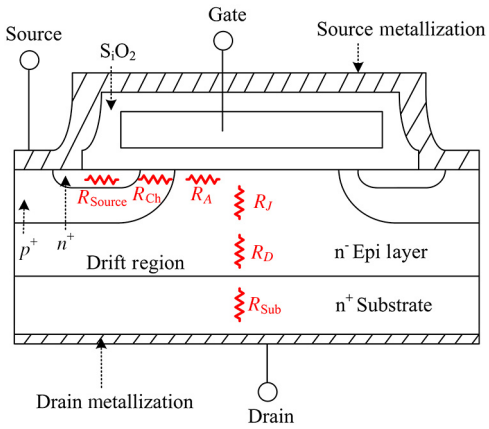

Fig. 1. Typical MOSFET structure with resistance components.

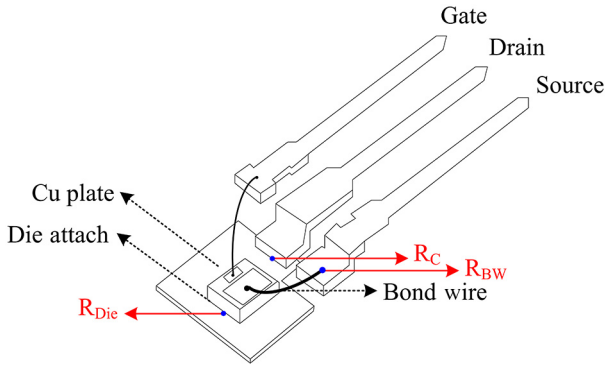

Fig. 2. Weak points of MOSFETs.

II. Aging Test-Bed for Thermal Cycling

A. Failure Mechanisms Due to Electrothermal Stress

Power MOSFET has a complex structure with differently doped n and p layers. In high-voltage MOSFETs, n layer has been further divided into two layers that are doped with high and low concentrations, to be able to withstand high forward voltage. A typical MOSFET structure showing the resistances of each layer and region from source-to-drain terminals is illustrated in Fig. 1. The total ON-state resistance of a power device is the sum of the individual resistances of each layer and region, and can be expressed as follows:

$$R_{\text{ds,on}} = R_{\text{Source}} + R_{\text{Ch}} + R_J + R_A + R_D + R_{\text{Sub}} + R_{\text{wcml}} \tag{1}$$

where R_{Source} is the source diffusion resistance, R_{Ch} is the channel resistance, R_A is the accumulation resistance, R_J is the resistance of the JFET region, R_D is the drift region resistance, and R_{Sub} is the n^+ substrate resistance. The rest of the resistances detailed in Fig. 2, which include the resistances of the bond wires (R_{BW}), metallization and contact resistances (R_C), and die attach solder resistances (R_{Die}), are denoted by R_{wcml}. In high-voltage MOSFETs, major contributing components of the $R_{\text{ds,ON}}$ are R_D and R_J, respectively. The remaining layer and channel resistances are relatively smaller, while R_{wcml} is generally negligible. Nevertheless, these contact points of different materials exhibit different thermal expansion characteristics due to different coefficients of thermal expansion (CTE). As a result of the induced tensile/compressive and shear stresses, they form the weak points of the power devices.

The applied shear stress is in direct relation with the contact surface. Thus, die attach solder joints having a large contact area carry high potential for failure [20]. On the other hand, the contact area of bond wires is quite small, yet, it has a direct connection to the active area of the FET. Because of this reason, large temperature swings can be observed at the joints. Large CTE mismatch and thermal swings make bond wires another potential weak point in the FET structure. When a power device is exposed to thermoelectrical stresses such as high mean temperature and large temperature swings, fatigues such as cracks, delamination, or complete lift-offs can occur at the above-mentioned weak points.

TABLE I
Failure Mechanisms With Respect to Stress Types

Failures mechanism	**Stress type**
Bond wire (cracks, lift-off)	T swing magnitude, mean T, T slope
Solder joint (voids/delamination)	T swing magnitude, mean T, T slope, humidity
Metallization (Al reconstruction)	T swing magnitude, mean T

* T: temperature.

In order for more reliable power converters, failure tests and reliability data are necessary during the development stage. However, these devices are meant to last for millions of cycles under normal and ideal operating conditions. To accelerate the fatigue process, accelerated aging tests are widely recognized, and had been demonstrated by many research groups. The majority of the package-related failures happen due to the electrothermal stresses. The type of the electrothermal stresses that trigger various types of failure mechanisms have been summarized in Table I [21].

B. Aging Test-Bed for Thermal Cycling

As it can be seen from Table I, main reasons behind the package-related failures are the temperature swing magnitude, slope, and mean temperature. In order to observe the effects of electrothermal stresses in a shorter time, accelerated thermal or power cycling tests are applied on custom-designed test-beds. In this work, a test-bed capable of applying thermal cycles to multiple discrete power MOSFETs through independently controlling their temperatures is presented [12]. The photograph of the designed built test-bed is given in Fig. 3.

The aforementioned failures, particularly die attach solder joint degradation, cause noticeable increment in the ON-state resistance. Since the individual resistance components are not measurable or sensible without decapsulation of the mold compound, researchers have observed and evaluated the variation of the total ON-state resistance of a power MOSFET [11]–[13], [15]. In the built accelerated test-bed, the measurements are taken in favor of finding out $R_{\text{ds,ON}}$ of the switches. Thus, each V_{DS} and I_D are sensed and transmitted to data acquisition system (DAQ), together with T_c.

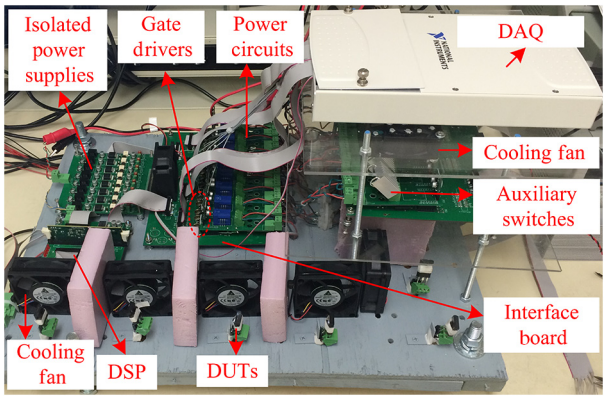

Fig. 3. Custom-built accelerated aging setup.

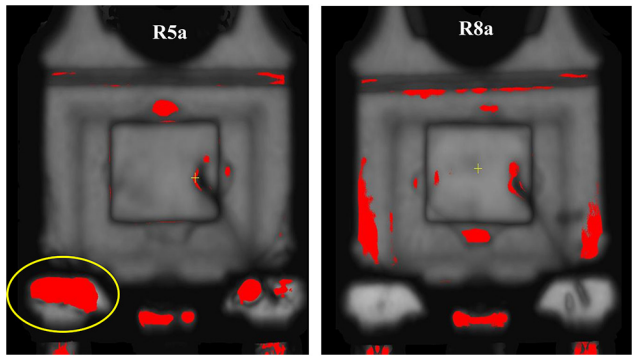

Fig. 4. C-SAM results of switches R5a and R8a.

The power circuit consists of series connected diode, current sensor, and the device under test (DUT). It is intended to use the power devices as the main load without adding an external load. In this test, the power supply is operated as a current source by limiting its current to the desired value. This helps to avoid current control loops in the DSP. When the switch is turned on, the adjusted current heats the device (active heating). In a similar manner, when the switch is turned off, no current passes through the device and cooling fans are engaged on.

The test-bed is designed for thermal cycling of discrete power switches, in which the temperature swing amplitude of each switch is controlled independently. K-type thermocouples are attached to the base plate of the switches and case temperature is fed to the DSP. The estimated junction temperatures are compared with the defined maximum and minimum temperature references, and a hysteresis band is developed in software for every switch.

III. Experimental Results of ON-State Resistance

A. Under Cyclic Thermal Stress

Two sets of tests are performed with different thermal swing amplitudes on 11-A/400-V power MOSFETs. In the first set of experiments, the switches are degraded under three different thermal conditions, which are: 1) $\Delta T_j = 160^\circ\mathrm{C}$ $T_{j\,\max} = 240^\circ\mathrm{C}$; 2) $\Delta T_j = 140^\circ\mathrm{C}$ $T_{j\,\max} = 220^\circ\mathrm{C}$; and 3) $\Delta T_j = 130^\circ\mathrm{C}$ $T_{j\,\max} = 210^\circ\mathrm{C}$, at a drain current of 5.2 A. In this particular test, the thermal swing amplitude is chosen high to shorten the duration of the tests. The elevated junction temperatures accelerate the aging mechanisms, particularly the gate-oxide degradation, due to the increased amount of trapped charges. In addition, the increased sheet resistance contributes to the measured $R_{\mathrm{ds,ON}}$, yet; the major root cause of the increased ON-state resistance is the die attach degradation. The trapped charges in the gate oxide and deformation on the upper metallization layer affect the other characteristics of the device more, such as gate threshold voltage, gate current, and leakage current.

It should be noted that measurements are taken at every five thermal cycles at the room temperature in order to make sure that device junction temperature remains the same in every measurement. However, the ON-state resistance measurement is quite challenging particularly when the converter is running, due to its dependence on junction temperature and drain current. Nevertheless, the measurements can be taken at the startups or zero crossings of the current to eliminate some of these dependencies as discussed in [22].

The experiments typically take several days to few weeks. The experimental results of eight of the switches are presented and analyzed in this paper, which are labeled as R1a–R2a and R4a–R9a.The most common observed failure was the loss of gate control. It should be highlighted that only R5a and R7a have failed during the experiments. The other switches were able to turn-on and turn-off; however, exhibited unstable $R_{\mathrm{ds,ON}}$. The devices aged to this level can be classified as "faulty," as the characteristics deviate from nominal values. R1a and R2a were functional and no abnormalities have been observed in these devices except increased $R_{\mathrm{ds,ON}}$.

The C-SAM results of the switches R5a and R8a are given in Fig. 4. C-SAM results are essential for finding out the voids/cracks or delamination at different surfaces. The red spots accompanied by the unexpected frequency responses observed at the surfaces are the indicators of voids and possible delamination. R5a has been identified as a failed device as previously discussed. This conclusion is also suggested by the C-SAM results. Deformation, possibly a delamination, can be observed at the contact surface of gate metal of R5a. In contrary, no sign of deformation is observed at the gate metal of R8a. Furthermore, the degraded switches are decapsulated to observe any potential damage on the die surface, as shown in Fig. 5, yet, no damage is observed other than the signs of metallization deformation and possible gate-oxide degradation, which potentially might have caused shifts in threshold voltage and the increase in the ON-state resistance.

The results of the online $\Delta R_{\mathrm{ds,ON}}$ measurements for the first set of experiments are given in Fig. 6. It is clearly seen that even though the same thermal swing is applied to the same type of switch from the same vendors, the degradation curves are slightly different. It is also observed that even slight increment in the thermal swing amplitude results in a distinctive end of life (EOL) cycle. This can be observed from samples R1a and R2a, where the EOL cycle is considerably more than that of samples R4a–R9a. It is found that degradation curve is in the form of an exponential function to some extent and a safe threshold can be determined for RUL estimation.

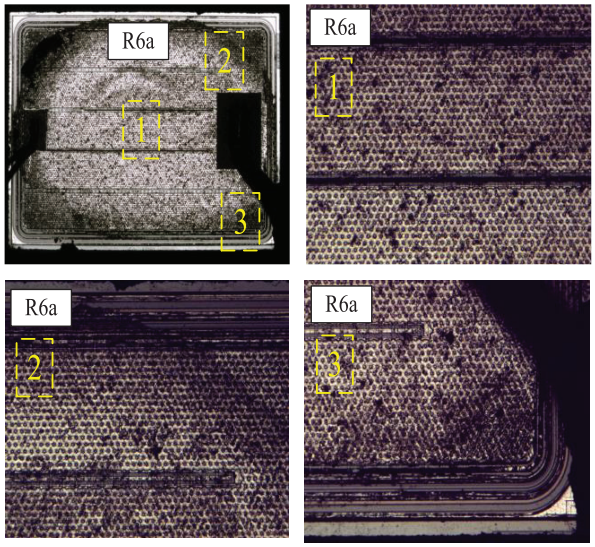

Fig. 5. Results of decapsulation of the switch R6a.

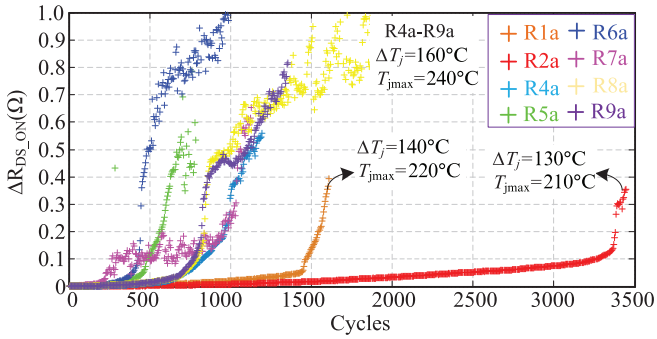

Fig. 6. Online $\Delta R_{\mathrm{ds,ON}}$ monitoring during thermal cycling under three different conditions. 1) $\Delta T_j = 160°\mathrm{C}\ T_{j\,\max} = 240°\mathrm{C}$. 2) $\Delta T_j = 140°\mathrm{C}\ T_{j\,\max} = 220°\mathrm{C}$. 3) $\Delta T_j = 130°\mathrm{C}\ T_{j\,\max} = 210°\mathrm{C}$.

The second set of experiments intends to degrade switches thermally with a swing amplitude of 80°C and a maximum junction temperature of 160°C. The experiments took approximately three weeks. This set of experiments is important to find out if similar results can be populated within shorter time. Similar to the results of the previous experiments, the $R_{\mathrm{ds,ON}}$ variation is found to be exponential to a certain value, each one exhibiting slightly different propagations under the same thermal conditions. The change in $R_{\mathrm{ds,ON}}$ is plotted in Fig. 7 for each switch till the degradation curve does not evolve exponentially anymore.

B. Under Variable Thermal Stress

The previous experimental results have been performed for cyclic thermal stress, where the thermal swing amplitude has been kept constant throughout the aging. In order to observe the ON-state variation under thermal swings with variable amplitudes, another test has been performed on the same power MOSFET, which experienced 10 consecutive thermal cycles of different amplitudes, as given in Fig. 8. The number of thermal swings that the switch experiences are $N_{\Delta Tj=110°\mathrm{C}} = 2$, $N_{\Delta Tj=120°\mathrm{C}} = 5.5$, $N_{\Delta Tj=130°\mathrm{C}} = 3$, and $N_{\Delta Tj=140°\mathrm{C}} = 0.5$. Please note that a thermal swing is defined as a complete

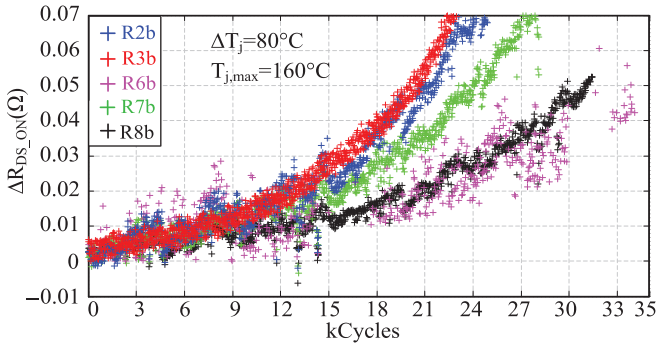

Fig. 7. Online $\Delta R_{\mathrm{ds,ON}}$ monitoring during thermal cycling at $\Delta T_j = 80°\mathrm{C} T_{j\,\max} = 160°\mathrm{C}$.

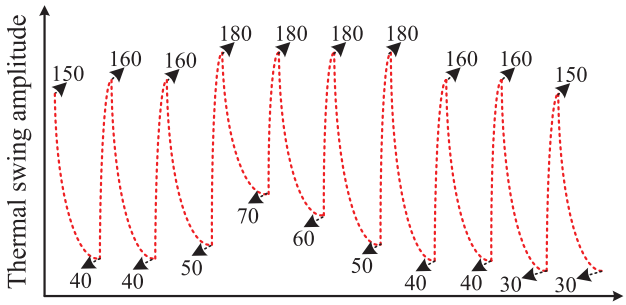

Fig. 8. Applied variable thermal swings.

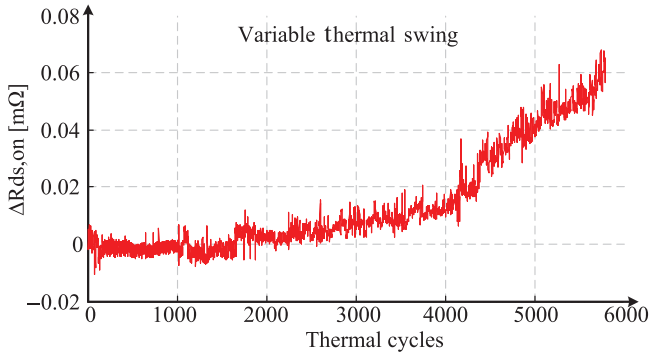

Fig. 9. ON-state resistance variation under variable amplitude thermal swings.

cycle (up and down). The experimental results of $\Delta R_{\mathrm{ds,ON}}$ are presented in Fig. 9. As it can be seen from the figure, the aging curve is again exponential and the accumulated damage is similar to that observed in tests where the thermal swing amplitude is 120°C.

IV. RUL Estimation Based on Palmgren–Miner Method

A. Coffin–Manson Model

The EOL of a power device can be modeled by the well-known Coffin–Manson model as given in (2), even though it has some shortcomings as it only considers the amplitude of the junction temperature, ΔT_j and the mean temperature T_m [23], [24]

$$N_f = \Delta T_j{}^{\delta} A e^{\frac{E_a}{kT_m}} \tag{2}$$

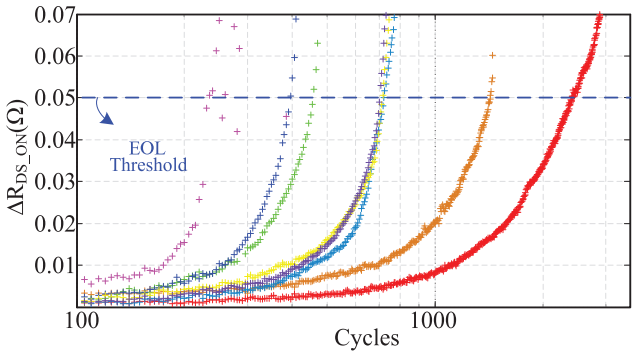

Fig. 10. Zoom-in profile of the degradation curve given in Fig. 6.

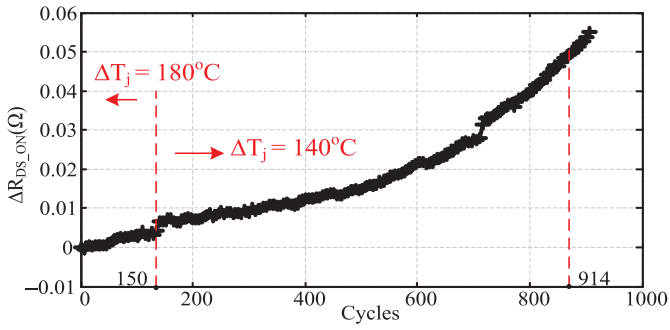

Fig. 11. Experimental results of ON-state resistance variation when ΔT_j is reduced from 180°C to 140°C at 150 cycles.

where E_a and k denote the thermal activation energy and Boltzmann constant in (2), respectively, while A and δ are the empirical constants. Due to its lack of physical information on the die and the packaging, (2) only provides a rough estimate of EOL for the switches.

The EOL of the switches can be determined by analyzing the zoom-in profile of the ON-state resistance variations given in Fig. 6. This logarithmic plot shown in Fig. 10 exhibits an exponential variation up to a certain value in the degradation process. Here, EOL is defined as 50 mΩ (12%) deviation from its initial ON-state resistance value that is chosen as the lowest threshold value for safety critical applications after exhaustive experiments.

In order to find the empirical constants in (2) for the aged MOSFETs, the results of two different test conditions can be expressed as

$$N_{f1} = \Delta T_{j1}{}^{\delta} A e^{\frac{E_a}{kT_{m1}}} \tag{3}$$

$$N_{f2} = \Delta T_{j2}{}^{\delta} A e^{\frac{E_a}{kT_{m2}}}. \tag{4}$$

Taking the natural logarithm of the above equations yields

$$\log(N_{f1}) = \delta \log(\Delta T_{j1}) + \log(A) + \frac{E_a}{kT_{m1}} \tag{5}$$

$$\log(N_{f2}) = \delta \log(\Delta T_{j2}) + \log(A) + \frac{E_a}{kT_{m2}}. \tag{6}$$

Thus, δ is found as

$$\delta = \frac{\log\left(\frac{N_{f2}}{N_{f1}}\right) - \frac{E_a}{k}\left(\frac{1}{T_{m2}} - \frac{1}{T_{m1}}\right)}{\log\left(\frac{\Delta T_{j2}}{\Delta T_{j1}}\right)}. \tag{7}$$

The empirical constant A can be found by substituting (7) into (3) as

$$A = e^{y} \tag{8}$$

where

$$y = \log(N_{f1}) - \delta \log(\Delta T_{j1}) - \frac{E_a}{kT_{m1}}. \tag{9}$$

By using test conditions $\Delta T_{j1} = 130°\text{C}$ $T_{j\max 1} = 210°\text{C}$ $N_{f1} = 2410$ and $\Delta T_{j2} = 160°\text{C}$ $T_{j\max 2} = 240°\text{C}$ $N_{f2} = 750$, the empirical coefficients for δ and A are calculated as -5.2776 and 4.9283×10^{13}, respectively. The found empirical coefficients are validated using a third test condition, $\Delta T_j = 140°\text{C}$ $T_{j\max} = 220°\text{C}$, and comparing the calculated EOL value with the experimental results. The calculated N_f is 1586 cycles for this case, whereas the actual experimental data suggest 1430 cycles. For more accurate result, advanced models taking the physical measures such as bond-wire diameter, etc. should be utilized. Even though the calculated result based on the simple model proposed in [24] does not perfectly match with the experimental data, it provides an insight on the range of N_f.

B. Lifetime Estimation Palmgren–Miner Linear Damage Accumulation Rule

The remaining lifetime with respect to thermal swing amplitude and corresponding EOL can be approximately calculated by Palmgren–Miner linear damage accumulation rule as [25]–[28]

$$\text{RL} = 1 - \sum_{1}^{n} \frac{N_n}{N_{\text{EOL,n}}}\bigg|_{\Delta T j_n} \tag{10}$$

where n represents the number of different thermal swing amplitudes experienced by the switch, N_n denotes the number of thermal swings experienced at thermal swing amplitude n, and $N_{\text{EOL},n}$ is the EOL found by the Coffin–Manson model for thermal swing amplitude n. The thermal cycles can be counted by rain-flow algorithm [17], [18], [29].

In order to illustrate the estimation of RUL using Palmgren–Miner linear damage accumulation rule, which accounts the number of thermal swings and thermal swing amplitudes, another switch has been thermally cycled with ΔT_j of 180°C for 150 cycles. After 150 cycles, the thermal cycle amplitude has been reduced to 140°C. The device has reached $\Delta R_{\text{ds,ON}}$ of 50 mΩ after 914 cycles, after which is considered as failed device. The resultant degradation curve is presented in Fig. 11. Using the Coffin–Manson model, the EOL is calculated as 371 cycles at $\Delta T_j = 180°\text{C}$. Likewise, the EOL is calculated as 1396 cycles at $\Delta T_j = 140°\text{C}$. The remaining lifetime can be calculated using (10). The estimation error is calculated as 4.8% with respect to the experimental results. Based on the obtained results, the Palmgren–Miner linear damage accumulation rule together with rain-flow counting algorithm can be

used to estimate the lifetime extension in real time. The drawback of this method is the necessity of junction temperature information.

C. Challenges in Junction Temperature Estimation for Aged Devices

The junction temperature can be estimated by monitoring electrothermal sensitive parameters such as saturation voltage [30] and threshold voltage [31] variations. Among these parameters, ON-state resistance of power MOSFETs and IGBT saturation voltage greatly varies due to aging in solder attachments and electrical resistances at contact points. On the other hand, threshold voltage is not affected by solder degradation and can be used to estimate the junction temperature if there is no degradation on the gate-oxide layer [31].

In high-power modules, a p-n junction mounted next to the Si chip can be monitored to sense the temperature [32]. This method is used in some industrial applications; however, it is suitable for very high-power module structure. The conventional way to estimate junction temperature is: 1) calculating the power losses at each step; 2) multiplying the losses with the thermal impedance; and 3) adding the generated heat in the device to the case temperature [33]–[35]. However, due to the solder degradation and thereby change in the thermal impedance, the estimated junction temperature may not be accurate.

V. Proposed RUL Estimation Based on On-State Resistance Variation

A. Exponential Degradation Model

The degradation growth can be modeled from the experimental data due to lack of information on the physical modeling of the device. As it can be observed from Figs. 7 and 10, the $R_{\mathrm{ds,ON}}$ increases exponentially with respect to thermal cycles in the defined RUL estimation zone with an initial value R_{init}. Thus, the degradation process can be modeled with an exponential curve, and an added offset value as

$$R_{\mathrm{ds,on}}(t) = \alpha e^{\beta t} + R_{\mathrm{init}}. \tag{11}$$

Assuming α and β as constants, (11) can be written in state-space form as

$$\dot{R}_{\mathrm{ds,on}}(t) = \left(R_{\mathrm{ds,on}}(t) - R_{\mathrm{init}}\right)\beta. \tag{12}$$

Discretizing the system yields

$$R_{\mathrm{ds,on}}(k+1) = R_{\mathrm{ds,on}}(k) \cdot (1 + \Delta t\beta) - R_{\mathrm{init}}\beta\Delta t. \tag{13}$$

This can be written in canonical form as

$$\begin{aligned} x(k+1) &= Ax(k) + Bu(k) \\ y(k) &= Cx(k). \end{aligned} \tag{14}$$

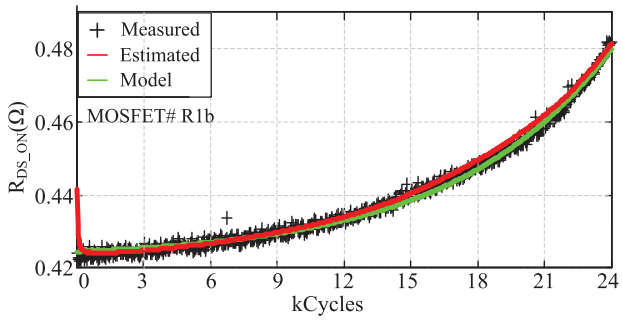

Fig. 12. Comparison of estimated trajectory and trajectory obtained from degradation model for the actual measurements of #R1b.

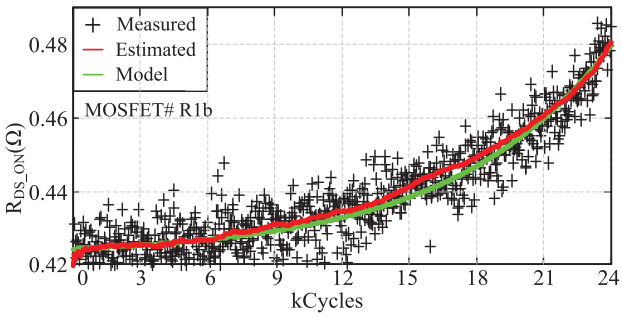

Fig. 13. Comparison of estimated trajectory and trajectory obtained from degradation model for the white noise added measurements of #R1b.

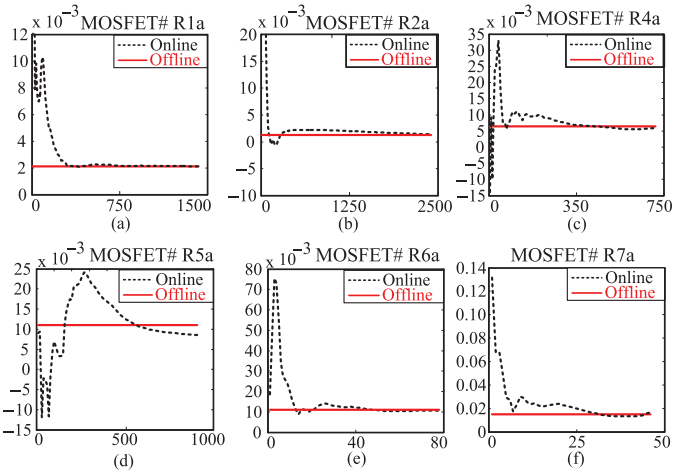

Fig. 14. Online β tracking for the samples. (a) #R1a. (b) #R2a. (c) #R4a. (d) #R5a. (e) #R6a. (f) #R7a.

B. Kalman Filter

It is possible to estimate the posterior state by applying KF to the empirical model given in (13). KF is a widely acknowledged optimal state estimator assuming a Gaussian distribution through minimizing the mean square error (mse) of the estimates considering the errors in the measurements and the model [36]

$$\begin{aligned} x_k &= Ax_{k-1} + Bu_k + w_k \\ Z_k &= \mathrm{H}x_k + v_k \end{aligned} \tag{15}$$

where w_k and v_k denote the process and measurement noises, respectively. The noise terms are assumed to be white and they

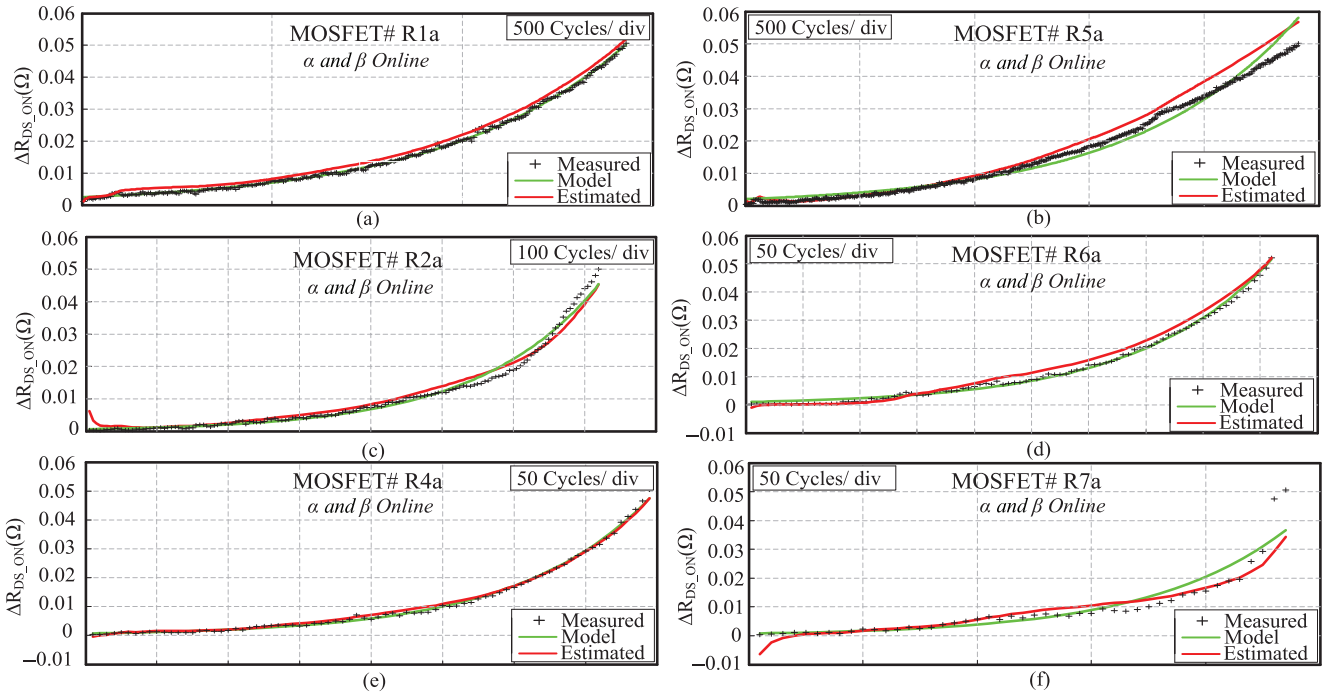

Fig. 15. State estimation with online computed α and β.

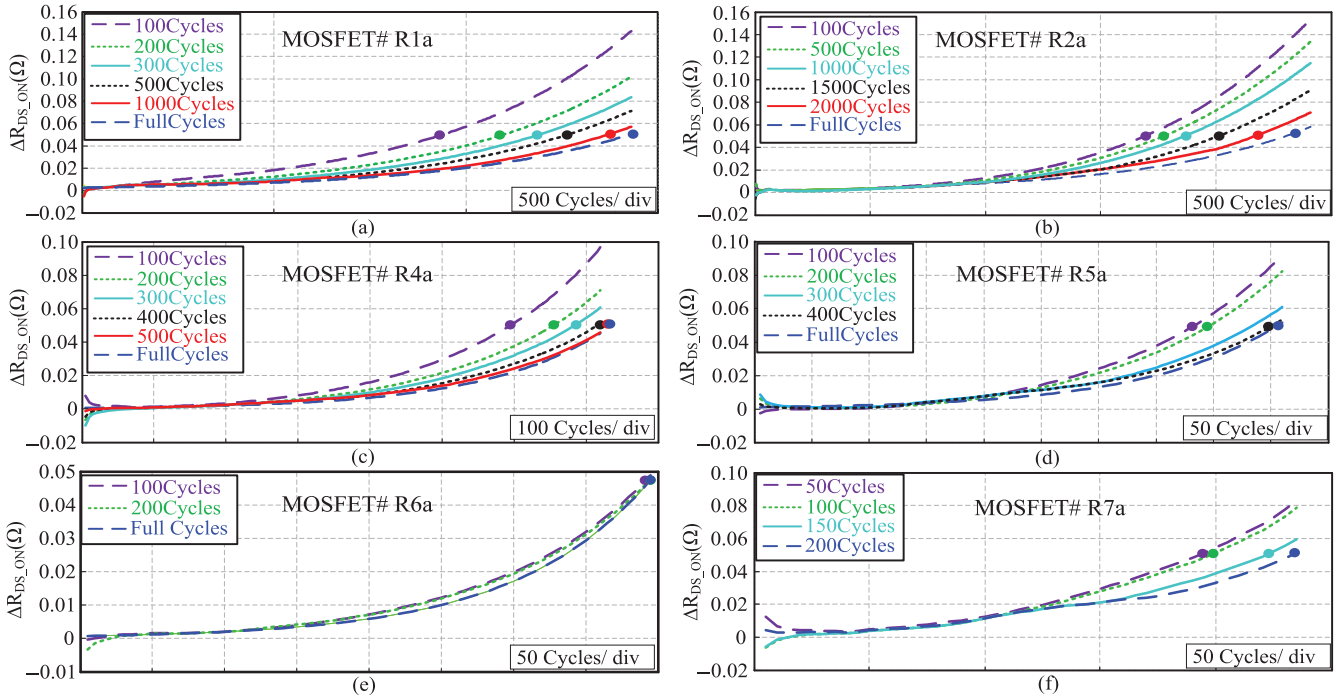

Fig. 16. RUL estimation for the samples #R1a, #R2a, and #R4a–#R7a with online computed α and β.

have Gaussian distribution with zero mean and the following covariance:

$$Q_k = E\left[w_k {w_k}^T\right] \tag{16}$$

$$R_k = E\left[v_k {v_k}^T\right]. \tag{17}$$

In the following equation, the estimation error covariance P_k is defined as the covariance of the difference between the true state at time k X_k and posterior state estimate $\hat{X}_k$:

$$P_k = \text{cov}\left[X_k - \hat{X}_k\right]. \tag{18}$$

The KF is defined for a discrete system as given in (15). The time updates of the KF for the priori state estimate and priori error covariance estimate are given as

$$\hat{X}_k^- = A_k \hat{X}_{(k-1)} + B_k u\,(k) \tag{19}$$

$$P_k{}^-\,(k) = A_k P_{(k-1)} {A_k}^T + Q_k. \tag{20}$$

TABLE II
RUL ESTIMATION OF THE SWITCHES WITH RESPECT TO THERMAL CYCLES

R#	Cycles	RUL ($R_{ds,th}$=50 mΩ)	RUL online α and β	Error online α and β%	RUL constant α and β	Error constant α and β%
R1a	100	1430	935	34.6	1020	28.7
	200	1430	1100	23.1	1180	17.5
	300	1430	1190	16.8	1230	14
	500	1430	1265	11.5	1275	10.8
	1000	1430	1370	4.2	1380	3.5
R2a	100	2410	1715	28.9	1720	28.6
	500	2410	1775	26.4	1775	26.4
	1000	2410	1875	22.2	1865	22.6
	1500	2410	2015	16.4	2015	16.4
	2000	2410	2170	9.9	2170	9.9
R4a	100	720	675	6.25	665	7.7
	300	720	695	3.5	700	3.5
	400	720	715	0.7	725	0.7
R5a	100	460	415	9.8	415	9.8
	200	460	385	16.3	405	11.2
	300	460	435	5.5	440	4.4
	400	460	450	2.2	445	3.2
R6a	100	395	400	1.2	440	4.4
	200	395	410	3.75	445	3.2

The measurement update involves the calculation of optimal Kalman gain, posterior state estimate, and posterior error covariance, which are expressed as

$$K_k = P_k{}^- H_k{}^T \text{inv}\left(H_k P_k{}^- H_k{}^T + R_k\right) \tag{21}$$

$$\hat{X}_k = \hat{X}_k^- + K_k\left(Z_k - \text{H}\hat{X}_k^-\right) \tag{22}$$

$$P_k = \left(I - K_k H_k\right) P_k{}^-. \tag{23}$$

At every time step, the new state is estimated in a recursive manner using the previous posterior estimate that is found through the time and measurement updates. The estimated trajectory using KF and trajectory obtained from the developed model is compared with the actual measurement data obtained from #Rb1 in Fig. 12. α and β are found through least-squares method evaluating all of the data points, where $\alpha = 0.001676$, and $\beta = 0.0001611$. In the results given in Fig. 13, a random white noise with a standard deviation of 0.005 is added on top of the measurement data. In this case, KF deals with the measurement noise and has no impact on finding the empirical coefficients.

C. Online α and β Computation

From Figs. 12 and 13, it is clear that fault growth trajectory of the degraded switches can be estimated within sufficient error margin, when α and β are computed using all the data points. This case is used as a benchmark as outlier effect is minimal when all data points are evaluated. However, when data points up to current time are computed with least-squares method to find α and β, the RUL prediction would be erroneous particularly at the beginning due to the effect of the outliers. In order to make the estimation online and robust, the data are filtered with KF at every time step and empirical coefficients are found based on this filtered data using least-squares method. The exponential curve can be written in the form as in (11), ignoring the initial value. Taking the natural logarithm of both sides yields

$$\ln \Delta R_{\text{ds,on}} = \ln \alpha + \beta x. \tag{24}$$

The best fit values for (24) are

$$a = \frac{\sum_{i=1}^{n} \ln y_i \sum_{i=1}^{n} {x_i}^2 - \sum_{i=1}^{n} x_i \sum_{i=1}^{n} x_i \ln y_i}{n \sum_{i=1}^{n} {x_i}^2 - \left(\sum_{i=1}^{n} x_i\right)^2} \tag{25}$$

$$b = \frac{n \sum_{i=1}^{n} x_i \ln y_i - \sum_{i=1}^{n} x_i \sum_{i=1}^{n} \ln y_i}{n \sum_{i=1}^{n} {x_i}^2 - \left(\sum_{i=1}^{n} x_i\right)^2} \tag{26}$$

where

$$\alpha = e^a \tag{27}$$

$$\beta \cong b. \tag{28}$$

In this fit, small $\Delta R_{\text{ds,ON}}$ values in (24) gets higher weights; thus, the following function should be minimized to distribute the weights equally among the points:

$$\sum_{i=1}^{n} y_i (\ln y_i - a - b x_i)^2. \tag{29}$$

Equation (29) can be minimized by using least squares method, which yields

$$a = \frac{\sum_{i=1}^{n} {x_i}^2 y_i \sum_{i=1}^{n} y_i \ln y_i - \sum_{i=1}^{n} x_i y_i \sum_{i=1}^{n} x_i y_i \ln y_i}{\sum_{i=1}^{n} y_i \sum_{i=1}^{n} {x_i}^2 y_i - \left(\sum_{i=1}^{n} x_i y_i\right)^2} \tag{30}$$

$$b = \frac{\sum_{i=1}^{n} y_i \sum_{i=1}^{n} x_i y_i \ln y_i - \sum_{i=1}^{n} x_i y_i \sum_{i=1}^{n} y_i \ln y_i}{\sum_{i=1}^{n} y_i \sum_{i=1}^{n} {x_i}^2 y_i - \left(\sum_{i=1}^{n} x_i y_i\right)^2}. \tag{31}$$

Using (27), (28) (30), and (31), it is possible to estimate α and β online using KF filtered data. It is also clear from the equations that α and β would converge with more data points.

D. RUL Estimation

The proposed KF integrated with the online exponential fitting of α and β are tested using the experimental data obtained from the first set of tests. Here, the characteristic variable is the β, which converges after approximately one-fifth of the total cycles, as shown in Fig. 14. Similarly, α converges around the same number of cycles. The outputs of the KF using the online computed α and β are given in Fig. 15. As it can be seen from the figures, the KF successfully filters and estimates the trajectory of the state.

Using the computed α and β up to current time step, it is possible to predict the RUL of the degraded switch till the threshold value is reached. To test the proposed algorithm, RUL of the samples R1a, R2a, and R4a–R7a are evaluated and the RULs are estimated at different cycle points. The results of the estimation are given in Fig. 16, and the RUL values along with estimation errors for online and offline computed α and β are summarized in Table II. For instance, the RUL of the sample R1a is estimated after 100 cycles as 935 and 1020 when online and offline computed α and β are used, respectively. The estimation errors are 34.6% and 28.7%, respectively. As the real measurements are taken, the error covariance is updated and trajectory converges to the one obtained from the model. With more data points, the estimation error reduces to 4.2% and 3.5%, respectively.

VI. Conclusion

The literature on counting the junction temperature cycles and estimating the EOL through Palmgren–Miner and Coffin–Manson models is well established. However, these methods require junction temperature information. In this paper, RUL estimation is targeted based on the recent findings on the ON-state resistance variation of power MOSFETs without using junction temperature information.

The safe RUL threshold value for the tested switch is determined as $50\ \mathrm{m}\Omega$, corresponding to 12% of its initial value. It is found that the ON-state resistance increases exponentially as switches undergo aging. This aging trend is modeled with an exponential empirical model. The empirical coefficients are found through least-squares algorithm run on KF filtered data, and RUL is estimated at different stages of aging. It has been shown that the error is minimized as more data points are evaluated. The findings on degradation and results suggest that the proposed real-time RUL estimation method can be utilized for failure prognostics.

Acknowledgment

The authors would like to thank Priority Labs for providing the failure analysis results that form the basis of this work.

References

[1] A. Lahyani, P. Venet, G. Grellet, and P.-J. Viverge, "Failure prediction of electrolytic capacitors during operation of a switchmode power supply," *IEEE Trans. Power Electron.*, vol. 13, no. 6, pp. 1199–1207, Nov. 1998.

[2] Y.-M. Chen, H.-C. Wu, M.-W. Chou, and K.-Y. Lee, "Online failure prediction of the electrolytic capacitor for LC filter of switching-mode power converters," *IEEE Trans. Ind. Electron.*, vol. 55, no. 1, pp. 400–406, Jan. 2008.

[3] G. M. Buiatti, J. A. Martín-Ramos, C. H. R. Garcia, A. M. R. Amaral, and A. J. Marques Cardoso, "An online and noninvasive technique for the condition monitoring of capacitors in boost converters," *IEEE Trans. Instrum. Meas.*, vol. 59, no. 8, pp. 2134–2143, Aug. 2010.

[4] K. Li, G. Y. Tian, L. Cheng, A. Yin, W. Cao, and S. Crichton, "State detection of bond wires in IGBT modules using eddy current pulsed thermography," *IEEE Trans. Power Electron.*, vol. 29, no. 9, pp. 5000–5009, Sep. 2014.

[5] S. Yang, D. Xiang, A. Bryant, P. Mawby, L. Ran, and P. Tavner, "Condition monitoring for device reliability in power electronic converters: A review," *IEEE Trans. Power Electron.*, vol. 25, no. 11, pp. 2734–2752, Nov. 2010.

[6] W. Kexin, D. Mingxing, X. Linlin, and L. Jian, "Study of bonding wire failure effects on external measurable signals of IGBT module," *IEEE Trans. Device Mater. Rel.*, vol. 14, no. 1, pp. 83–89, Mar. 2014.

[7] V. Smet *et al.*, "Ageing and failure modes of IGBT modules in high-temperature power cycling," *IEEE Trans. Ind. Electron.*, vol. 58, no. 10, pp. 4931–4941, Oct. 2011.

[8] H. Oh, B. Han, P. McCluskey, C. Han, and B. D. Youn, "Physics-of-failure, condition monitoring, and prognostics of insulated gate bipolar transistor modules: A review," *IEEE Trans. Power Electron.*, vol. 30, no. 5, pp. 2413–2426, May 2015.

[9] N. Patil, J. Celaya, D. Das, K. Goebel, and M. Pecht, "Precursor parameter identification for insulated gate bipolar transistor (IGBT) prognostics," *IEEE Trans. Rel.*, vol. 58, no. 2, pp. 271–276, Jun. 2009.

[10] B. Ji, V. Pickert, W. Cao, and B. Zahawi, "In situ diagnostics and prognostics of wire bonding faults in IGBT modules for electric vehicle drives," *IEEE Trans. Power Electron.*, vol. 28, no. 12, pp. 5568–5577, Dec. 2013.

[11] J. Celaya, A. Saxena, P. Wysocki, S. Saha, and K. Goebel, "Towards prognostics of power MOSFETs: Accelerated aging and precursors of failure," in *Proc. Annu. Conf. Prognostics Health Manage. Soc.*, 2010, pp. 1–10.

[12] S. Dusmez and B. Akin, "An accelerated thermal aging platform to monitor fault precursor on-state resistance," in *Proc. IEEE Int. Elect. Mach. Drives Conf. (IEMDC'15)*, May 10–13, 2015, pp. 1–6.

[13] A. Sow, S. Somaya, Y. Ousten, J. Vinassa, and F. Patoureaux, "Power MOSFET active power cycling for medical system reliability assessment," *Microelectron. Rel.*, vol. 53, no. 9–11, pp. 1697–1702, Sep./Nov. 2013.

[14] G. Sonnenfeld, K. Goebel, and J. R. Celaya, "An agile accelerated aging, characterization and scenario simulation system for gate controlled power transistors," in *Proc. IEEE AUTOTESTCON*, 2008, pp. 205–215.

[15] J. R. Celaya, P. Wysocki, V. Vashchenko, S. Saha, and K. Goebel, "Accelerated aging system for prognostics of power semiconductor devices," in *Proc. IEEE AUTOTESTCON*, 2010, pp. 1–6.

[16] J. R. Celaya, A. Saxena, S. Saha, and K. Goebel, "Prognostics of power MOSFETs under thermal stress accelerated aging using data-driven and model-based methodologies," in *Proc. Annu. Conf. Prognostics Health Manage. Soc.*, 2011, vol. 2, pp. 1–10.

[17] H. Huang and P.A. Mawby, "A lifetime estimation technique for voltage source inverters," *IEEE Trans. Power Electron.*, vol. 28, no. 8, pp. 4113–4119, Aug. 2013.

[18] L. R. GopiReddy, L. M. Tolbert, B. Ozpineci, and J. Pinto, "Rainflow algorithm based lifetime estimation of power semiconductors in utility applications," *IEEE Trans. Ind. Appl.*, vol. 51, no. 4, pp. 3368–3375, Jul./Aug. 2015.

[19] Y. Zheng, L. Wu, X. Li, and C. Yin, "A relevance vector machine-based approach for remaining useful life prediction of power MOSFETs," in *Proc. Prognostics Syst. Health Manage. Conf. (PHM'14 Hunan)*, Aug. 24–27, 2014, pp. 642–646.

[20] M. Ciappa, "Selected failure mechanisms of modern power modules," *Microelectron. Rel.*, vol. 42, no. 4–5, pp. 653–667, 2002.

[21] P. Ghimire, S. Bęczkowski, S. Munk-Nielsen, B. Rannestad, and P. B. Thøgersen, "A review on real time physical measurement techniques and their attempt to predict wear-out status of IGBT," in *Proc. IEEE Power Electron. Appl. Conf.*, 2013, pp. 1–10.

[22] S. Dusmez and B. Akin, "An active life extension strategy for thermally aged power switches based on pulse-width adjustment method in interleaved converters," *IEEE Trans. Power Electron.*, vol. 31, no. 7, pp. 5149–5160, Oct. 2015.

[23] I. F. Kovacevic, U. Drofenik, and J. W. Kolar, "New physical model for lifetime estimation of power modules," in *Proc. Int. Power Electron. Conf. (IPEC'10)*, 2010, pp. 2106–2114.

[24] S. S. Manson, *Thermal Stress and Low Cycle Fatigue*. New York, NY, USA: McGraw-Hill, 1966.
[25] M. Musallam, C. Yin, C. Bailey, and M. Johnson, "Mission profile-based reliability design and real-time life consumption estimation in power electronics," *IEEE Trans. Power Electron.*, vol. 30, no. 5, pp. 2601–2613, May 2015.
[26] M. A. Miner, "Cumulative damage in fatigue," *J. Appl. Mech.*, vol. 67, pp. A159–A164, 1945.
[27] S. Suresh, *Fatigue of Materials*. Cambridge, U.K.: Cambridge Univ. Press, 1991, p. 133.
[28] A. Fatemi and L. Yang, "Cumulative fatigue damage and life prediction theories: A survey of the state of the art for homogeneous materials," *Int. J. Fatigue*, vol. 20, no. 1, pp. 9–34, 1998.
[29] M. Musallam and C. M. Johnson, "An efficient implementation of the rainflow counting algorithm for life consumption estimation," *IEEE Trans. Rel.*, vol. 61, no. 4, pp. 978–986, Dec. 2012.
[30] Z. Arbanas, "High power density 1 MW motor inverter," in *Proc. IEEE Int. Elect. Mach. Drives Conf. (IEMDC'97)*, May 1997, pp. WB1/2.1–WB1/2.2.
[31] H. Chen, B. Ji, V. Pickert, and W. Cao, "Real-time temperature estimation for power MOSFETs considering thermal aging effects," *IEEE Trans. Device Mater. Rel.*, vol. 14, no. 1, pp. 220–228, Mar. 2014.
[32] T. Kajiwara, A. Yamaguchi, Y. Hoshi, K. Sakurai, and J. Gallagher, "New intelligent power module - chip modules with junction temperature detection function," in *Proc. 33rd IEEE IAS Annu. Meeting Ind. Appl. Conf.*, Oct. 1998, pp. 1085–1090.
[33] F. W. Gutzwiller and T. P. Sylvan, "Power semiconductor ratings under transient and intermittent loads," *Trans. Amer. Inst. Elect. Eng.—Commun. Electron.*, vol. 79, no. 6, pp. 699–706, Jan. 1961.
[34] S. K. Ghandhi, *Semiconductor Power Devices Physics of Operation and Fabrication Technology*. Hoboken, NJ, USA: Wiley, 1977, pp. 301–306.
[35] G. L. Skibinski and W. A. Sethares, "Thermal parameter estimation using recursive identification," *IEEE Trans. Power Electron.*, vol. 6, no. 2, pp. 228–239, Apr. 1991.
[36] S. Dusmez and B. Akin, "Remaining useful lifetime estimation for degraded power MOSFETs under cyclic thermal stress," in *Proc. IEEE Energy Convers. Congr. Expo. (ECCE'15)*, Sep. 2015, pp. 3846–3851.

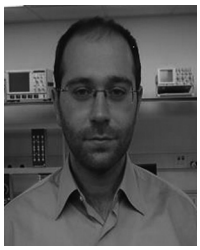

Serkan Dusmez (S'11) received the B.S. (with honors) and M.S. degrees in electrical engineering from Yildiz Technical University, Istanbul, Turkey, in 2009 and 2011, respectively, and the M.S. degree in electrical engineering from Illinois Institute of Technology, Chicago, IL, USA, in 2013. Currently, he is working toward the Ph.D. degree at The University of Texas at Dallas, Richardson, TX, USA.

From 2012 to 2013, he was a Faculty Research Assistant with the Power Electronics, Energy Harvesting, and Renewable Energies Laboratory, Department of Electrical and Computer Engineering, University of Maryland, College Park, MD, USA. He has authored/coauthored over 45 journal and conference papers. His research interests include design of power electronic interfaces and energy management strategies for renewable energy sources, integrated power electronic converters for plug-in electric vehicles, and real-time fault diagnosis of power converters.

Mr. Dusmez was the recipient of the 2015 Best Vehicular Electronics Paper Award from the IEEE Vehicular Technology Society, the 2014–2015 Louis Beecherl Jr. Graduate Fellowship, and the 2015–2016 Ericsson Graduate Fellowship from The University of Texas at Dallas.

Hamit Duran (M'06) received the M.S. degree in electrical engineering from ETH Zurich, Zurich, Switzerland, in 1988, and the Ph.D. degree in physics from the Institute for Quantum Electronics, ETH Zurich, in 1995.

In 1995, he joined the Institute for Business and Production Management (BWI), ETH Zurich, where he was a Postdoctoral Researcher, working on chip-on-board and multichip module technology and conducted postgraduate studies in business and production management. From 1997 to 1998, he was leading the R&D Department, AMEDA AG, Huenenberg, Switzerland, a Swiss manufacturer of products for breastfeeding applications, neonatology (newborns), and suction pumps for medical use. In 1999, he joined Philips Semiconductors, Zurich, as Assembly Engineering Manager, where he was in charge of the world-wide assembly and packaging activities of all products developed in Zurich which included SMD and BGA packages, system-in-package (SiP), and chip-on-foil packages (COFs). In 2006, he joined ABB Switzerland where he held various positions. Among others, he was in charge of research and development in the field of packaging and semiconductors for power electronics applications at the ABB Corporate Research Center. Later on, he was the Head of the BiMOS Modules Product Technology Department including R&D, application, and production testing groups at ABB Semiconductors. In 2014, he joined Texas Instruments, Dallas, TX, USA, where he is in charge of strategy, roadmap, and competitive assessment for high-voltage and high-power packaging.

Dr. Duran was the Chapter Chair of the IEEE Switzerland CPMT Chapter from 2009 to 2014.

Bilal Akin (S'03–M'08–SM'13) received the B.S. and M.S. degrees in electrical engineering from Middle East Technical University, Ankara, Turkey, in 2000 and 2003, respectively, and the Ph.D. degree in electrical engineering from Texas A&M University, College Station, TX, USA, in 2007.

From 2005 to 2008, he was an R&D Engineer with the Toshiba Industrial Division, Houston, TX, USA. From 2008 to 2012, he was an R&D Engineer with the C2000 Embedded Control Group, Texas Instruments Incorporated, Dallas, TX, USA. Since 2012, he has been an Assistant Professor with The University of Texas at Dallas, Richardson, TX, USA. His research interests include design, control, and diagnosis of electric motors and drives, digital power control and management, and fault diagnosis and condition monitoring of power electronics components and ac motors.

Dr. Akin is an Associate Editor of the IEEE TRANSACTIONS ON INDUSTRY APPLICATIONS and the IEEE TRANSACTIONS ON VEHICULAR TECHNOLOGY. He was the recipient of a 2015 NSF CAREER Award, Jonsson School Faculty Research Award, and Top Editors Recognition Award from the IEEE TVT Society.